Effect of adsorptive fouling on membrane performance: case study with a pulp mill effluent

Dal-Cin, M. M.; Striez, C. N.; Tweddle, T. A.; Capes, C. E.; McLellan, F.; Buisson, H.

Publisher's version / Version de l'éditeur:
https://doi.org/10.1016/0011-9164(95)00018-W
Desalination, 101, 2, pp. 155-167, 1995

ELSEVIER

Desalination 101 (1995) 155–167

DESALINATION

Effect of adsorptive fouling on membrane performance: Case study with a pulp mill effluent*

M.M. Dal-Cin[a**], C.N. Striez[a], T.A. Tweddle[a], C.E. Capes[a], F. McLellan[b], H. Buisson [c]

[a]*National Research Council of Canada, Institute for Environmental Research and Technology, Ottawa, Canada*
[b]*Abitibi-Price, Sheridan Park Technology Center, Mississauga, Ontario, Canada*
[c]*Wastewater Technology Center, Burlington, Ontario, Canada*

Received 5 June 1994; accepted 8 September 1994

Abstract

The compatibility of a wide range of membrane materials with a pulp mill effluent was evaluated with respect to adsorptive fouling. Membranes were initially evaluated by their pure water permeability and separation characteristics with a polyethylene glycol test solute. These membrane coupons were contacted with a pulp mill effluent sample at 50°C in the absence of a transmembrane pressure for 3 h and then recharacterized. The change in the separation and permeation was interpreted as changes in the average pore size and the ratio of the number of pores to the effective pore length ($n/\Delta xA$) of the membrane. A decreasing pore size indicated the formation of an adsorbed fouling layer. An increased $n/\Delta xA$ ratio suggested that adsorption occurred on the membrane surface rather than in the pores.

Keywords: Fouling; Adsorption; Ultrafiltration; Pulp mill waste

1. Introduction

This work was part of a comprehensive study on the fouling of membranes during ultrafiltration (UF) of a pulp mill effluent. Membrane fouling is currently a major limiting factor to the full-scale application of membrane technology in many areas. In the resource sector membrane technology has a potential role in alleviating pollution problems. In particular, the pulp and paper industry has been under increasing legislation regarding emissions. The

*Issued as NRCC No. 37572.

**Corresponding author.

SSDI 0011-9164(95)00018-6

viability of membrane technology in this sector is directly linked to the cost of implementation in comparison to other competing technologies such as biological treatment. This is particularly important when considering pollution control, as there is little or no recovered costs as in the biotechnology, pharmaceutical or food industries. These have high value products that can offset the cost of membrane systems. There is a need to advance the understanding and control of membrane fouling during UF in order to improve the competitiveness of membrane processes. This can help to minimize the cost of implementation and increase the acceptance of membrane technology on an industrial scale.

In this paper, one particular aspect of membrane flux decline is systematically studied. A wide variety of membrane materials and pore sizes was characterized by their permeability and separation characteristics. Membranes were exposed to a plug screw feeder pressate (PSFP) from a semi-chemical mechanical pulp (SCMP) mill and then recharacterized to quantify changes in the membrane's morphology. A steric transport model was used to estimate the membrane's pore size. This pore size was used to evaluate the ratio of the number of pores to the effective pore length per unit area ($n/\Delta xA$) of the membrane. Changes in these two parameters were used to interpret the mechanism of adsorptive fouling.

2. Flux models

Flux losses during UF occur through various mechanisms including: adsorption, steric hindrance, pore plugging and concentration polarization or gel layer formation [1,2]. These contributions have been modelled phenomenologically using series resistance (SR) models [3] or combined osmotic pressure-adsorption (OPA) models [1]. Flux models may have the general form

$$PR = \frac{(\Delta P - \sigma\pi)}{\mu\left(R_m + R_a + R_{pp} + R_h\right)} \quad (1)$$

where PR is the product rate, ΔP the transmembrane pressure drop, π the osmotic pressure of the feed solution at the membrane-solution interface, σ the reflection coefficient and μ the permeate viscosity. R_m, R_a, R_{pp} and R_h are the resistances to permeate flow due to the membrane, adsorptive fouling, pore plugging and concentration polarization or gel layer formation, respectively.

The purely resistance models do not make use of the osmotic pressure term, accounting for this effect with R_h. Alternatively, osmotic pressure models will use the $\sigma\pi$ term to account for the reduced driving force and may represent the effects of other fouling mechanisms with the individual components or an overall fouling term, R_f. Regardless of the model used, the adsorptive fouling component has been recognized as a significant factor in flux decline [4–6].

The effect of adsorptive fouling can be estimated by comparing pure water permeabilities (*PWP*s) before and after contacting experiments. Increased adsorptive fouling during permeation is a distinct possibility. This would result from more of the membrane's internal pore structure being exposed to foulants and higher concentrations at the membrane surface due to polarization. However, permeation experiments would confound the flux loss due to adsorptive fouling and pore plugging. Separate contacting and permeation experiments would therefore allow estimating both R_a and R_{pp} as separate resistances and is the subject of further work continuing fouling studies with PSFP.

The pore restriction model has also been used to model adsorptive fouling [7–9]. This model predicts a narrowing of pore sizes due to adsorption of solutes on the membrane surface and pore walls. The flux decline has a fourth-

order dependence on the pore radius as described by Hagen-Pouiseille flow. An estimate of an adsorbed layer of uniform thickness (l_a) can be obtained from the initial pore size (r_i) and the relative flux, RF, of the new and fouled membrane:

$$l_a = r_i \left[1 - \left[\frac{PWP_f}{PWP_i} \right]^{0.25} \right] = r_i \left(1 - RF^{0.25}\right) \quad (2)$$

Eq. (1) can be rearranged to obtain

$$1 - RF^{0.25} = \frac{l_a}{r_i} \quad (3)$$

which predicts a straight line with a slope of l_a when $(1 - RF^{0.25})$ is plotted as a function of $1/r_i$.

Dejmek and Nilsson [9] evaluated adsorption of several proteins on polysulfone membranes to distinguish whether adsorptive fouling was occurring on the surface or on pore walls. They used the hypothesis that surface adsorption would result in an adsorptive resistance which was independent of the initial flux, while pore restriction would depend on PWP_i as predicted by Eq. (2). They concluded that pore restriction best described their results. However, the pore restriction model is not appropriate for use in all cases of adsorptive fouling, and its shortcomings have been described by Persson et al. [10]. The validity of the pore restriction model depends on the relative sizes between the solute(s) and pores. Meireles et al. [4] and Belfort et al. [11] clearly demonstrated the different cases which may be encountered (Fig. 1) during UF of protein solutions. This analysis can also be applied to the case of purely adsorptive fouling. Brink et al. [12] have described the adsorption of surfactants on membranes in a similar manner.

When the pore size is considerably smaller than the foulant (Fig. 1a), the pore size of the membrane remains unchanged. Since the foulants are much larger than the pores, the spaces between the foulants will be larger than the pores. The formation of the adsorbed layer adds a hydraulic resistance resulting in flux losses. At the opposite extreme, when the pore size is much larger than the foulant (Fig. 1b), the foulant enters the pore, adsorbing on the pore walls and reducing the effective pore size. Fluxes decrease — as would be expected — due to the reduced flow area and represent the situation for which the pore restriction model is best suited. At some intermediate pore sizes (Fig. 1c), the foulants mask the membrane's pores and establish new separation characteristics determined by the size of the foulants, as was shown by Meireles et al. [4]. Once again, the hydraulic resistance increases, resulting in flux reductions.

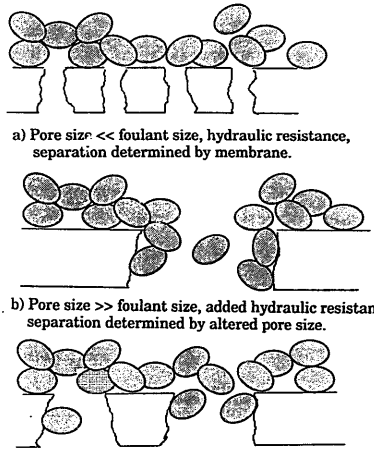

Fig. 1. Schematic representation of adsorption mechanisms on/in the membrane pore structure showing the effect of the relative sizes of the foulant and pore.

In the intermediate case, the new effective molecular weight cut-off (MWCO) of the membrane was shown to be a function of the size of the adsorbed foulant. The pore size was determined by the intermolecular spaces and increased with increasing foulant size. The pore size distribution was also considerably narrower. This would be expected as the foulants were virtually monodispersed, resulting in similar intermolecular openings.

3. Materials

The feed material used for the adsorption study was the PSFP from an SCMP mill. This effluent is a complex mixture of resin and fatty acids (RFAs), soluble and insoluble lignins, simple organic acids, sugars, fine wood fibres and polysaccharides. The composition of PSFP is summarized in Tables 1 and 2. Samples were collected during regular operation of the pulp mill, screened with a 400-mesh sieve and refrigerated at 2°C until used.

A wide range of membrane materials and pore sizes was evaluated to determine their adsorptive fouling characteristics. Membranes were obtained from commercial manufacturers or produced with an automated casting machine in our laboratories. The membrane materials tested are summarized in Table 3; individual membranes will be highlighted in later discussions.

Table 1
Molecular weight distribution of PSFP

Molecular weight	Dissolved solids, wt%	Total organic carbon, wt%
<1 K	52	42
1 K < mw < 3K	18	20
3 K < mw < 30 K	1	↑
30 K < mw < 100 K	3	38
>100 K	26	↓

Membranes were characterized using 6000 Da polyethylene glycol (6 K PEG) as a test solute. The PEG was used as purchased from Fluka with a claimed molecular weight distribution of 5000–7000 Da. Characterization solutions were prepared with a concentration of 200 ppm PEG in reverse osmosis (RO) water.

4. Experimental

Membranes were characterized at 3.4 bar (50 psi), a cross-flow velocity of 0.8 m/s at 25°C using thin channel test cells with an effective surface area of $14.5\times10^{-4}m^2$ as described by Hazlett et al. [13]. The cross-flow velocity corresponds to a Reynolds number of ~800. The geometry of the cell causes the feed to impinge normal to the plane of the membrane. This flow pattern and the short travel path promote mixing at the membrane surface beyond that suggested by the Reynolds number. The low test solute concentration and cell design minimize concentration polarization which would bias estimates of the pore size.

Membrane coupons were first characterized by their *PWP* after 5 h permeation with RO feed water. This ensured complete removal of any residual solvents and/or storage media.

Table 2
Composition of unfiltered PSFP

pH	5.7
Electrical conductivity, μΩ	5,100
Dissolved solids, mg/l	12,600
Suspended solids, mg/l	1,700
Total organic carbon, mg/l	5,670
Biological oxygen demand, mg/l	5,250
Resin and fatty acids, mg/l	432
Lignin sol, mg/l	2,400
Lignin insol, mg/l	1,900
Volatile acids, mg/l	920
Sugars, mg/l	2,680

Table 3
Average *RF* of various membrane materials after contacting PSFP for 3h at 50°C

Material	No. of samples	*RF*			
		Average (%)	SD (%)	Minimum (%)	Maximum (%)
Teflon	1	274			
TFCs	9	130	75	21	237
Reg cell	11	99	11	82	113
Modified PVDF	8	97	39	42	146
Olefin	1	95			
CA	9	91	35	36	149
Sulfonated PS	1	39			
PVDF	8	78	28	38	119
PAN	6	70	23	43	106
PAI	9	58	29	12	93
CTA	7	53	31	12	88
Acrylic	2	49	22	33	64
PS	20	41	33	7	134
PEI	8	30	11	13	44
Modified PS	8	29	24	6	68
PES	10	22	12	8	48
PA	4	21	15	9	41

Separations were evaluated using 6 K PEG and RO water was then recirculated until the PEG concentration was reduced to <2 ppm. Membrane coupons were removed from the test cells and contacted with the effluent on both surfaces at 50°C for 3 h with gentle stirring at 1 h intervals. This temperature was selected as it is the expected operating temperature of a full-scale installation. Membrane coupons were rinsed under RO water for ~1 min on both sides and reinstalled in the test cells. The *PWP* with RO water and 6 K PEG separation characteristics were then redetermined. Concentrations of the feed and permeate were determined with a Shimadzu 5000 TOC analyzer.

5. Membrane characterization

The PEG separations were used to estimate the pore size using a single parameter (r_p) radially averaged pore model according to Tremblay [14]

$$f = 1 - \frac{\chi}{1 - e^{-Pe}(1-\chi)} \tag{4}$$

The pore Peclet number, *Pe*, is the ratio of the convective and diffusive transport of the solute through the pore. Both types of solute flow account for the influence of the pore wall as the solute size approaches the pore size. A global steric parameter (χ) associated with the restricted convective transport within the pore and the ratio of restricted diffusivity (ξ) of the solute within the pore to the bulk diffusivity of the solute are calculated numerically [15]. The Peclet number can be defined as

$$Pe = \frac{\chi}{\xi D_\infty}\left[\frac{r_p^2 \Delta p}{8\mu}\right] \tag{5}$$

The viscosity of water is μ and ΔP is the pressure drop across the membrane.

A parameter characterizing the combined effects of a membrane's porosity and resistance to flow can be obtained from the pure water permeation rate once the pore radius (r_p) has been determined from the 6 K PEG solute sieving experiments [16]. Rearranging the Hagen-Poiseuille equation, a ratio of the number of pores (n) to the pore length (Δx) per unit area (A) can be obtained:

$$\frac{n}{\Delta x A} = \frac{8Q\mu}{\pi \Delta P r_p^4 A} \tag{6}$$

This ratio is a convenient measure of a membrane's performance for a given pore size. Using the pore size and $n/\Delta xA$ provides more information regarding changes at the membrane surface than would be possible using the MWCO and *PWP*.

6. Results and discussion

6.1. Relative pure water flux and membrane materials

From a practical point of view, the *RF* provides a clear measure of the effects of adsorptive fouling with PSFP. The *RF*s for various membrane materials are summarized in Table 3 and indicate the average *RF*, standard deviation, minimum and maximum *RF* values and the number of coupons tested. The large number of coupons, manufacturers and pore sizes evaluated in several classes of materials made identification of each membrane impractical.

A large range of *RF*s is immediately evident, from ~20% to almost 300%, with considerable variability for some materials. This may stem from the nature of the experiments, testing of single coupons and various membrane preparation methods from the different manufacturers. Despite this, the ranking of materials largely follows expected trends, the most hydrophobic materials having the lowest *RF*.

Fluorinated polymers such as Teflon (polytetrafluoroethylene) have low surface energy and would be expected to exhibit little or low adsorption. However, it was not clear what adsorptive fouling, if any, may have occurred with the Desalination Systems, Inc. K150 Teflon membrane tested (0.1 μm). The PWP_f increased to 274% of the PWP_i after exposure to PSFP. The increased *PWP* may have been due to only partial removal of storage media. The *PWP* increased from 30 to 147 $l/m^2/h$ during the 5 h preconditioning and so the high *RF* may have been a continuation of this trend. Polyvinylidene fluoride (PVDF) has chemical properties similar to Teflon; it would be expected to adsorb more material due to the presence of $-CH_2$ groups. These membranes had an average *RF* of 78%, ranging from 38% to 119%. The range of *RF*s for the PVDF membranes and odd results with the Teflon membrane made comparisons between the two materials difficult.

Modified PVDF membranes showed a wide range of *RF*s after contacting with PSFP. This may be expected given that there were three manufacturers making this class of membranes, undoubtedly using different modifications. Poor reproducibility was obtained with the DDS ETNA series (1 K, 10 K and 20 K MWCOs). *RF*s of ~150% and ~60% were observed for the same pore sizes in replicate tests. Separations of 6 K PEG decreased by more than 20–30% when the *RF* was >100%. This suggests that the surface modification may be removed or degraded by PSFP. Past experience with these membranes in our laboratories has seen definite colour changes after use, from dark to light brown, suggesting a loss of the surface modification or coating. Similar observations have been made by researchers at Wastewater Technology Center.

The thin film composite (TFC) class of membranes also showed widely varying degrees of fouling resistance. As with the modified PVDF membranes, this was not unexpect-

ed as this class could consist of widely varying surface chemistries. The Desalination Systems Inc. G10 and G50 (2 K and 15 K MWCO, respectively) and Nitto Denko Corp. NTR 7410 (10% NaCl separation) are reported to be sulfonated polysulfones. Nitto Denko Corp. describes their NTR 729HF membrane as a polyvinylalcohol (PVA) derivative. Peterson [17] suggests that there is also polypiperazineamide present in the barrier layer along with the PVA. Desalination's DESAL 5 (200 MWCO) composition is unknown, although it may be a tri-laminate of polypiperazineamide on a sulfonated polysulfone on polysulfone [17].

Changes in their performance varied considerably after contacting with PSFP. The G10 and G50 fluxes increased beyond their *PWP*s while maintaining or increasing the separation of 6 K PEG. The *RF* for the DDS GS81 (6 K MWCO), which is a non-TFC-sulfonated membrane, was 39%, indicating severe adsorptive fouling. The *RF* for the NTR 729HF was >200% in replicate tests. Unlike the G10 and G50 membranes, 6 K PEG separations decreased from ~90% to ~50%, suggesting some change in the membrane surface morphology or properties.

Several TFC membranes had *RF*s >100% even though separations increased marginally. This does not imply that the membrane was degraded as the separations would have decreased in such a case. Membranes were pressurized with water for 5 h before testing, so *PWP* increases were unlikely to have been caused by washing away some sort of storage media, unless it was not highly water soluble as was suspected with the Teflon membrane. It is possible that the top layer of the composite membrane was partially removed by PSFP, but still left intact at the coating/support interface. This would have reduced the hydraulic resistance resulting in higher *PWP*s while the separation of 6 K PEG would have remained the same or increased if some PSFP remained on the surface. This mechanism is difficult to verify, but the observed behaviour is unlikely to be an anomaly given that it was largely restricted to coated membranes such as TFCs, modified PVDF and was reproducible with several membranes.

Cellulosic membranes were further subdivided into cellulose acetate (CA), cellulose tri-acetate (CTA) and regenerated cellulose (RC). The regenerated cellulosics all had extremely high *RF*s with a minimum of 90%, suggesting little or no adsorptive fouling. This was supported by the negligible changes in 6 K PEG separations. Some coupons had *RF*s slightly above 100%, which may have been due to experimental error, unlike the large increases discussed earlier. The low adsorptive fouling with regenerated cellulose membranes with PSFP is consistent with previously reported work using proteins such as BSA [1] and peptides [18].

The cellulose acetate and tri-acetate samples showed some variability in adsorption. The average cellulose acetate *RF* was 91%, largely due to the performance of four different MWCO membranes from Osmonics Inc. (S series with MWCOs of 2 K, 20 K, 50 K and 100 K). The remaining cellulose acetate membranes appeared to have somewhat lower *RF*s at ~53%. The tri-acetates fouled more than the other cellulosics. The increasing *RF* of the cellulosic membranes was consistent with the increasing hydrophilicity of materials and their composition: cellulose > cellulose acetate > cellulose tri-acetate. Cellulose tri-acetate was expected to be the most hydrophobic with three acetate groups.

Polyamide (PA), polysulfones (PS and PES) and polyether-imide (PEI) are considered to be hydrophobic materials which would exhibit severe adsorptive fouling. This was the case with *RF*s for each class of material ranging from 21% to 41%. High increases of 6 K PEG separation were observed with the low *RF*s for these materials. The modified polysulfones

tested had been typically used in biological applications where they had superior adsorptive fouling resistance. The low *RF*s exhibited with PSFP suggest that they are not compatible with this feed.

The *RF* of polyacrylonitrile (PAN) and polyamide-imide (PAI) membranes varied considerably. The *RF* of PAI membranes was loosely tied to the initial pore size, following the trend predicted by the pore size restriction model, while there was no obvious trend with the PAN membranes.

The range of *RF*s observed for a wide range of materials demonstrates the potential for adsorptive fouling to influence membrane performance with PSFP. Regenerated cellulose membranes from several manufacturers all exhibited very low fouling with respect to unaltered pore sizes and *RF*s. Several TFCs also appear compatible with PSFP although changes of membrane properties warrant further investigation.

6.2. Relative fluxes and pore size relationships

The pore restriction model predicts a diminishing relative flux loss as the pore size increases. This trend was not observed with any of the membrane materials due to large variations in the *RF* throughout the range of pore sizes. These variations may have been due to differences in manufacturing, storage media, additives, etc. of the suppliers. Membranes with a wide range of pore sizes were made in our laboratories [19] with PAI, PEI and PES, under similar conditions to study the relationship between adsorptive fouling and pore size.

The *RF* varied considerably for the PAI membranes, ranging from 12% to 93% (Table 4) and could not be correlated with the initial *PWP*, although the highest *RF*s were obtained with the most permeable membranes. Separations of 6 K PEG before contacting with PSFP were already near 100% for the tighter PAI membranes (1–4), making pore size changes undetectable. Separations for intermediate PAI membranes (5–7) approached similar levels (~85%) despite widely different initial separations.

A series of PES membranes also showed similar trends. Separations for membranes 1–6 increased to high levels (>80%) from initial levels as low as 7%. Several approached 100% separation; hence it is not known if the new

Table 4
Relative fluxes for PAI, PEI and PES membranes for increasing MWCOs (as indicated by the increasing *PWP* and decreasing 6 K PEG separation)

Material	PWP_i (l/m²/h)	*RF* (%)	PWP_f (l/m²/h)	6 K PEG separation (%)	
				Before	After
PAI:					
1	48	46	22	99	102
2	84	72	61	97	99
3	95	45	43	101	97
4	108	73	79	92	99
5	125	69	86	81	90
6	615	12	73	23	84
7	729	22	157	14	87
8	1474	93	1372	6	2
9	4887	90	4403	−1	0
PES:					
1	78	24	19	44	91
2	140	18	25	88	94
3	256	11	28	34	98
4	322	8	24	36	98
5	364	16	57	7	81
6	670	17	113	7	84
7	795	48	381	6	18
PEI:					
1	127	13	16	77	95
2	147	24	35	71	61
3	257	17	44	51	93
4	322	35	114	17	46
5	436	36	159	5	45
6	878	40	349	1	13
7	1047	31	329	4	48
8	1086	44	482	5	12

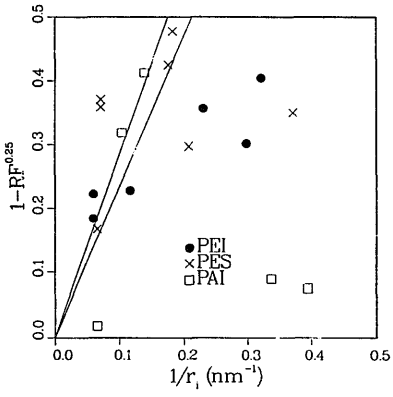

Fig. 2. $(1-RF^{0.25})$ plotted as a function of $1/r_i$ for PAI, PES and PEI membranes. The solid lines represent theoretical values for adsorbed layer thicknesses $2.35 < l_a < 2.85$ nm.

effective pore size was smaller than indicated. PWP_fs also approached a common value at ~25–30 l/m²/h. Membranes produced from PEI showed no trends with neither separations nor fluxes approaching a common level.

A quantitative analysis of the pore restriction model can be made using Eq. (3). Fig. 2 shows no correlation between $(1-RF^{0.25})$ and $1/r_i$ over the observed range of pore sizes for any of the materials. Estimates of the adsorbed layer thickness, l_a, can be obtained if the analysis is restricted to membranes with the largest pore sizes. It would appear that from Fig. 2 a straight line through the origin was plausible only for $1/r_i < 0.2$ nm^{-1}. A linear regression on these data gave adsorbed thicknesses of 2.35, 2.47 and 2.85 nm for PEI, PAI and PES, respectively. The upper and lower ranges of l_a are shown in Fig. 2 as solid lines. Given the scatter in the experimental data, the differences between l_a for the different materials should not be considered significant. The pore restriction model was adequate only for pore radii > 5.0 nm, which was in reasonable agreement with the adsorbed layer thickness. Smaller pores would result in the adsorbed layer bridging the pore rather than covering the interior pore wall.

The behaviour exhibited by the PES and PAI membranes can be described by the fouling mechanisms proposed by Meirles et al. [4] and Brink et al. [12]. The separation characteristics of membranes with intermediate pore sizes appear to be determined by the membrane after adsorptive fouling. The similar separations for 6 K PEG for intermediate membranes suggested that the separations were effected by the adsorbed layer. The similarity of the PWP_f for these membranes suggested that the fouling layer was a significant, if not the dominant, hydraulic resistance. This behaviour was not observed for membranes with large initial pore sizes, as would be expected from the discussion of Fig. 1.

6.3. Pore size and porosity effects

Changes in membrane morphology can also be examined more rigorously using the ratio $n/\Delta xA$ and pore size described earlier. PWP reductions are expected after adsorptive fouling but cannot distinguish between adsorptive fouling resulting in pore restriction, plugging or a continuous layer on the membrane surface. Fig. 3 shows how these parameters changed for PES membranes after adsorptive fouling. The membrane designation (e.g., PES-2) and arrowhead of the vector indicate the properties of the new and fouled membrane, respectively. All membranes showed a pore size reduction, as they must, based on the increased 6 K PEG separations described earlier. However, the increase in the ratio $n/\Delta xA$ was unexpected. These observations clearly contradict the pore restriction model which would predict either a constant or decreasing $n/\Delta xA$. This ratio would decrease either through total pore blockage (decreasing n) or by Δx increasing due to the

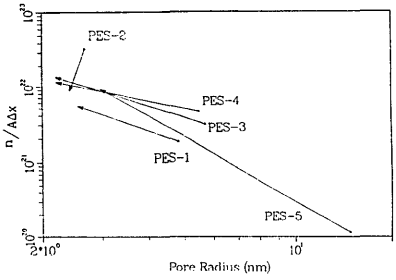

Fig. 3. Changes in PES membrane characteristics due to adsorptive fouling with PSFP.

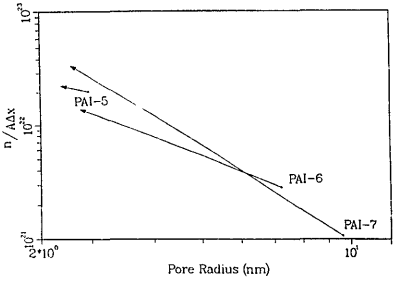

Fig. 4. Changes in PAI membrane characteristics due to adsorptive fouling with PSFP.

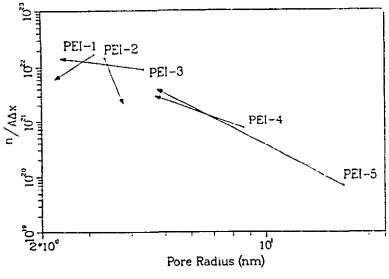

Fig. 5. Changes in PEI membrane characteristics due to adsorptive fouling with PSFP.

effective membrane thickness increasing by the adsorbed layer thickness, l_a. The new pore size and $n/\Delta xA$ reflect the properties of the new adsorbed layer. The mechanism of an adsorbed layer establishing new permeation characteristics is more likely and can account for $n/\Delta xA$ increasing, as was already demonstrated by Mereiles et al. [4] in Figs. 1a and 1c.

The use of a single solute to characterize the pore size limits the number of usable PAI membranes to three. Estimation of pore size changes with the other samples is difficult as the 6 K PEG separations were either nearly 100% or zero. The PAI membrane data presented in Fig. 4 show trends similar to those observed with the PES membranes, a reduction in the effective pore size and increasing $n/\Delta xA$.

Another feature of both the PES and PAI fouled membrane data is the similarity of fouled pore sizes, which follows from the similarity of the 6 K PEG separation data. The PES and PAI membranes have a fouled effective pore radius between 2.5–3 nm. This observation is also consistent with that predicted by Mereiles et al.

Mixed results were obtained with the PEI membranes. The ratio $n/\Delta xA$ decreased with two of the membranes and did not tend toward a common effective pore size (Fig. 5). This may suggest a different fouling mechanism from that of the PAI and PES membranes, such as pore plugging or pore restriction. This was unexpected as the initial pore size ranges for all three membrane materials were similar and all exhibited severe fouling.

6.4. Error analysis

The use of multiple PEG solutes for pore size estimation would have utilized a larger range of initial membrane pore sizes and allowed a more accurate estimation of the

Table 5
Variability of the membrane porosity parameter, $n/\Delta xA$, based on an error of ±5% on the 6 K PEG separation

Membrane		$\frac{n}{\Delta xA}$ range (m^{-3})		Pore radius range (nm)		Are changes significant?
		Clean	Fouled	Clean	Fouled	
PAI:	5	$1.59\text{-}2.67\times10^{22}$	$1.74\text{-}3.26\times10^{22}$	3.16- 2.77	2.81-2.40	Not significant
	6	$1.62\text{-}4.55\times10^{21}$	$1.08\text{-}1.85\times10^{22}$	8.31- 6.42	3.04-2.66	Significant
	7	$0.4\text{-}2.15\times10^{21}$	$2.7\text{-}4.8\times10^{22}$	12.3 - 8.08	2.92-2.53	Significant
PES:	1	$1.33\text{-}2.46\times10^{21}$	$4.06\text{-}7.82\times10^{21}$	5.21- 4.47	2.7 -2.35	Significant
	2	$2.56\text{-}4.58\times10^{22}$	$0.63\text{-}1.44\times10^{22}$	2.88- 2.49	2.66-2.16	Significant
	5	$0.08\text{-}3.79\times10^{20}$	$7.24\text{-}12.2\times10^{21}$	27.3 -10.5	3.16-2.77	Significant
PEI:	2	$1.14\text{-}1.87\times10^{22}$	$1.62\text{-}2.71\times10^{21}$	3.57- 3.16	4.06-3.57	Significant
	3	$0.68\text{-}1.19\times10^{22}$	$1.05\text{-}2.21\times10^{22}$	4.67- 4.06	2.69-2.24	Not significant
	4	$0.34\text{-}1.34\times10^{21}$	$2.22\text{-}4.03\times10^{21}$	10.5 - 7.41	5.05-4.35	Significant

changes in membrane properties. Nonetheless, these changes cannot be attributed to experimental error. The estimate of the pore size was calculated using Eq. (4) which is a complex function of the test solute to pore size ratio. The ratio $n/\Delta xA$ is inversely proportional to the fourth power of the pore size as predicted by the Hagen-Poiseuille relationship, making the determination of $n/\Delta xA$ sensitive to pore size estimates.

The significance of the changes in membrane morphology can be seen in Table 5. They were used as an alternative to error bars on $n/\Delta xA$ in Figs. 3-5 for the sake of clarity. The accuracy of the 6 K PEG separation data was generously assumed to be ±5%. Taking the upper and lower limits of the plausible range of separations, the equivalent pore sizes were estimated. These were used to determine a range of $n/\Delta xA$ values for a fixed PWP_i and PWP_f. Significant changes were taken to be those for which $n/\Delta xA$ values did not overlap. Only two cases were determined to be insignificant — PAI-5 and PEI-3. Figs. 3-5 showed several other cases where large increases of $n/\Delta xA$ were observed. These were not included as the assumption of ±5% error on the 6 K PEG separation data would have resulted in separations <0 or >100%. Similar increases of $n/\Delta xA$ were observed for numerous other membranes summarized in Table 3.

7. Conclusions

Adsorption or contacting tests were shown to provide qualitative information on adsorptive fouling of various membrane materials with PSFP. Materials were ranked on the basis of their relative flux, $RF=PWP_f/PWP_i$, after contacting PSFP in the absence of any transmembrane pressure. Ideal membrane materials based on these criteria were regenerated cellulose and various hydrophilic TFCs. Hydrophobic materials such as polysulfones, polyamide-imide and polyether-imide exhibited severe adsorptive fouling.

Increased pure water permeabilities after adsorption tests were observed for several TFCs, modified PVDF and surface-coated membranes. Test solute separations were often maintained in these situations suggesting that the membrane was not damaged. The increased pure water permeability may have resulted from further removal of storage media or partial removal of the surface modification,

lowering the hydraulic resistance of the membrane.

Estimates of the adsorbed layer thickness obtained from the pore restriction model ranged from 2.35 to 2.85 nm for a set of control membrane materials. This model appeared to be adequate for pore radii >5 nm, as expected for the estimated adsorption layer thickness.

Changes in the membrane's morphology described by the pore radius and the ratio $n/\Delta xA$ suggested adsorptive fouling on the surface of the membrane for pore radii <5 nm. The fouled membranes showed a tendency to a similar pore radius between 2.5–3 nm, indicating the formation of a new surface on the membrane whose pore size is determined by the adsorbed layer. The observed increases of $n/\Delta xA$ were inconsistent with adsorption in the membrane pores and could not be attributed to experimental error. The ratio $n/\Delta xA$ would be expected to decrease during pore restriction due to pore plugging (reduction of n) or an increase in the effective pore length Δx due to the adsorbed layer. The increased ratio $n/\Delta xA$ reflects the properties of the layer adsorbed on the membrane surface. This behaviour was consistent with changes in membrane morphology measured by Meireles et al. [4].

8. Symbols

A — effective permeation area of membrane, m^2
D_∞ — diffusivity of solute in solution, m^2/s
f — separation
l_a — thickness of the adsorbed layer, m
LMH — permeation rate, $l/m^2/h$
n — number of pores
Pe — Peclet number
PEG — polyethyleneglycol
PSFP — plug screw feeder pressate
PWP — pure water permeation rate, $(L)/m^2/d$
PWP_f — pure water permeation rate after adsorptive fouling, $(L)/m^2/d$
PWP_i — pure water permeation rate for a new membrane, $(L)/m^2/d$
ΔP — pressure drop across the pore, kPa
Q — volumetric flow rate, m^3/h
RF — percent relative flux, PWP_f/PWP_i
RFA — resin and fatty acids
R_j — hydraulic resistance of membrane, or resistance due to adsorption, pore plugging or concentration polarization, 1/m
r_p — pore radius, nm
r_i — pore radius of a new membrane, nm
SCMP — semi-chemical mechanical pulp
TOC — total organic carbon
Δx — effective length of the membrane pore, m

Greek

μ — viscosity, Pa· s
$\sigma\pi$ — reflection coefficient and osmotic pressure, Pa
ξ — ratio of restricted diffusion within the pore to free diffusion in bulk solution
χ — global steric parameter

9. Acknowledgements

The authors would like to thank Pritham Ramamurthy of the Pulp and Paper Research Institute of Canada, Ashwani Kumar and Chung Ming Tam of I.E.R.T. for helpful discussions, and Eric Chen for performing permeation experiments.

References

[1] M.K. Ko and J.J. Pellegrino, J. Membr. Sci., 74 (1992) 141.
[2] C.M. Tam and A.Y. Tremblay, J. Membr. Sci., 57 (1991) 271.
[3] A.S. Jonsson, J. Membr. Sci., 79 (1993) 93.
[4] M. Meireles, P. Aimar and V. Sanchez,, J. Membr. Sci., 56 (1991) 13.
[5] H.J. Hanemaaijer, T. Robbertsen, Th. van den Boomgaard and J.W. Gunnink, Desalination, 68 (1989) 199.
[6] L.E.S. Brink and D.J. Romijn, Desalination, 78 (1990) 209.
[7] A.M. Brites and M.N. de Pinho, J. Membr. Sci., 78 (1993) 265.
[8] J.R.V. Flora, J. Membr. Sci., 76 (1993) 85.
[9] P. Dejmek and J.L. Nilsson, J. Membr. Sci., 40 (1989) 189.
[10] K.M. Persson and J.L. Nilsson, Desalination, 80 (1991) 123.
[11] G. Belfort, J. Pimbley, A. Greiner and K.Y. Chung, J. Membr. Sci., 77 (1993) 1.
[12] L.E.S. Brink, S.J.G. Elbers, T. Robbertsen and P. Both, J. Membr. Sci., 76 (1993) 281.
[13] J.D. Hazlett, O. Kutowy and T.A. Tweddle, in Proc., 2nd Internat. Conf. Separations Sci. and Tech., M.H.I. Baird and S. Vijayan (eds.), Canadian Soc. for Chem. Engineering, Ottawa, 1989, pp. 65-74.
[14] A.Y. Tremblay, The role of structural forces in membrane transport: cellulose membranes, Ph.D. Thesis, University of Ottawa, 1989.
[15] J. Happel and H. Brenner, Low Reynolds Number Hydrodynamics, Martinus Nijhoff, Dordrecht, 1986.
[16] T.A. Tweddle, C.N. Striez, C.M. Tam and J.D. Hazlett, Desalination, 86 (1991) 27.
[17] R.J. Petersen, J. Membr. Sci., 83 (1993) 81.
[18] P. Mourot and M. Oliver, Sep. Sci. and Technol., 24(5,6) (1989) 353.
[19] C.M. Tam, M.M. Dal-Cin and M.D. Guiver, J. Membr. Sci., 78 (1993) 123.